5-2017

Compositionally Graded Indium Gallium Nitride Solar Cells

Christopher Matthews
University of Arkansas, Fayetteville

COMPOSITIONALLY GRADED
INDIUM GALLIUM NITRIDE SOLAR CELLS

COMPOSITIONALLY GRADED INDIUM GALLIUM NITRIDE SOLAR CELLS

A thesis submitted in partial fulfillment
of the requirements for the degree of
Honors Bachelor of Science
in Electrical Engineering

by

Christopher Matthews

May 2017
University of Arkansas

Abstract

For the past several decades, methods to harvest solar energy have been investigated intensively. A majority of the work done in this field has been on solar cells made with silicon – the most mature semiconductor material. Recent developments in material fabrication and processing techniques have enabled other semiconductor materials to attract practical interest and research effort as well. Indium gallium nitride (InGaN) is one such material. The material properties of InGaN indicate that solar cells made with it have the potential to achieve much higher power density than a standard silicon solar cell. High power density InGaN solar cells could replace silicon cells in applications where size and weight are critical, or in environments where silicon devices cannot survive. This is especially true of space, and most InGaN development has been done with that in mind. However, at high enough power densities, InGaN solar cells could begin to compete with silicon devices in commercial applications. The goal of this research is to investigate the effect a novel growth technique for InGaN – graded layer deposition – has on the power density of an InGaN solar cell.

In this research, first a baseline InGaN solar cell was grown, fabricated, and characterized. A standard PiN (P: p-type, i: intrinsic, N: n-type) structure was used for this baseline device. The reference alloy composition was chosen to be 20% indium and 80% gallium ($In_{0.2}Ga_{0.8}N$). This sample was grown using molecular beam epitaxy (MBE) under standard conditions for the material. Once the reference crystal was fabricated it was optically and electrically characterized. The material composition was verified through a combination of x-ray diffraction (XRD), photoluminescence (PL), and transmittance/reflectance measurements. The quality of the surface of the crystal was examined using atomic force microscopy (AFM). Once the optical characterization of the material was complete, the crystal was processed for electrical

characterization. Individual devices were constructed by etching away much of the p-type and intrinsic layer, leaving behind circular mesas. Each mesa was then given a top and bottom contact, so that it could be connected to test equipment electrically. After the crystal was processed into a solar cell in this way, each device was connected to a test source electrically, and the current-voltage (I-V) curves were taken. This information was used to find the current and power densities of each device.

The second step in this work was fabricating and characterizing a graded layer device that was similar to the reference cell. To this end, the graded layer device was chosen to have a starting composition of 25% indium and 75% gallium, with an ending composition of 15% indium and 85% gallium in place of the intrinsic layer. This new crystal was grown under identical conditions as the baseline cell, except for the graded layer, which required a slightly different approach. The graded layer crystal was then characterized and processed consistent with the reference in an attempt to get as accurate of a comparison between the two as possible. The results of this research could significantly affect the field of III-nitride solar cells.

Acknowledgments

I would like to thank Dr. Morgan Ware for his encouragement, mentorship, and guidance throughout this project. This work would not be possible if it were not for his efforts, as well as those of his graduate students: Pijush Ghosh, Mirsaeid Sarollahi, Malak Refaei, and Manal Aldawsari. Additionally, the help I received from Andrian Kuchak and Yang Wu for characterization was critical to the success of the project. Finally, Kelly McKenzie's patience and willingness to share resources as she scrambled to complete her thesis alongside me.

I could not have completed my degree, much less this thesis, without the support of my parents. A special thank you goes out to my amazing girlfriend, Stephanie Sandoval for staying awake with me many nights, providing moral support, making sure I ate, and keeping me sane.

Table of Contents

1. Introduction 1

1.1 Motivation 1

1.2 Thesis Statement 1

1.3 Organization of Thesis 2

2. Background 3

2.1 Properties of Indium Gallium Nitride 3

2.2 Molecular Beam Epitaxy 4

2.3 Photoluminescence, Reflectance & Transmittance 5

2.4 X-Ray Diffraction 6

2.5 Atomic Force Microscopy 7

3. Experimental Approach 8

3.1 Reference Cell 8

3.2 Graded Layer Cell 15

4. Experimental Results 17

4.1 Reference Cell 17

4.2 Graded Layer Cell 26

5. Conclusions 30

5.1 Discussion of Results 30

5.2 Suggestions for Future Work 30

References 32

List of Figures

Figure 1. Available energy in the solar spectrum compared to Si and III-nitride band gaps [1].... 4

Figure 2. Schematic view of MBE [7]. 5

Figure 3. XRD Schematic [11]. 6

Figure 4. AFM Schematic [12]. 7

Figure 5. (a) DHJ structure by Fabien, et. al. [13]. (b) Modified structure used as the reference cell. 8

Figure 6. Veeco Gen II MBE System. 9

Figure 7. Photoluminescence Setup. 10

Figure 8. Philips Diffractometer. 11

Figure 9. Shimadzu UV-3600 Reflectance Setup. 12

Figure 10. Bruker AFM. 13

Figure 11. Solar Cell Mask Set. 14

Figure 12. Graded Cell Structure. 15

Figure 13. Photoluminescence at 15K. 17

Figure 14. Photoluminescence at 50K. 18

Figure 15. Photoluminescence at 150K. 18

Figure 16. Photoluminescence at 250K. 18

Figure 17. Photoluminescence at 298K. 18

Figure 18. Reference Crystal ω-2Θ Scan. 19

Figure 19. Reference Crystal Reciprocal Space Map. 20

Figure 20. Reflectance Profile of Reference Crystal. 21

Figure 21. Derivative of Reflectance for Reference Crystal. 22

Figure 22. Transmittance of Reference Crystal. 22

Figure 23. Middle 25-µm^2 AFM (a) raw data. (b) software-flattened image. 23

Figure 24. Middle 400-µm^2 AFM. 24

Figure 25. I-V Plot – Reference Device C2R4. 25

Figure 26. Graded Layer 2Θ-ω Scan. 27

Figure 27. Reflectance of Graded Layer Crystal. 27

Figure 28. Derivative of Reflectance for Graded Layer Crystal. 28

Figure 29. Graded Layer 4-µm^2 AFM Results. 29

Figure 30. Graded Layer 25-µm^2 AFM Results. 29

List of Tables

Table 1. Titanium Etch Times. 13

Table 2. Reference Device Power Metrics. 25

1. Introduction

1.1 Motivation

Single-junction silicon solar cell development has begun to plateau, and increases in efficiency of these cells beyond 30% are projected to be minimal in the near future [1]. At this efficiency, photovoltaics are not competitive with oil-based energy. To continue improving on solar technology, with the goal of supplementing and eventually replacing fossil fuels, new materials and structures capable of boosting solar efficiency beyond the limit of silicon.

Solar cells have begun to be applied to fields outside of pure power generation, although that remains their purpose. It is often difficult to power electronics in harsh environments such as high and low temperature, high pressure, and highly radiated places. Silicon-based electronics, including solar cells, are ill-suited for use in these applications, and because of that solar energy has been eschewed. However, new robust materials have recently gained traction in the world of photovoltaics, and have opened the door for harsh environment solar generation.

1.2 Thesis Statement

The primary purpose of this thesis is to structurally characterize a graded indium gallium nitride (InGaN) solar cell, and compare it to a previously studied InGaN PiN (P: p-type, i: intrinsic, N: n-type) reference solar cell. A secondary objective of the project is to prepare the devices used for optical and electrical characterization. To accomplish the goals of this research, a reference crystal was grown by molecular beam epitaxy (MBE), and subsequently characterized by photoluminescence (PL), x-ray diffraction (XRD), reflectance, transmittance, and atomic force microscopy (AFM). Once characterized, the crystal was processed into a solar

cell, and a current-voltage sweep was conducted on the device. The graded layer device was fabricated and characterized in much the same way.

1.3 Organization of Thesis

The body of this thesis consists of five chapters. First, this Introduction presents the reasons that this research is worthwhile, a brief description of the goals and methods, and this map of the thesis. Next, the Background introduces the reader to the theory behind solar cells, the material of interest, and each technique used to produce results. Third, the Experimental Approach expounds on the methods listed in Section 1.2 and described in Chapter 2 for both the reference and graded cells. The Experimental Results chapter presents the results obtained from the approach described in Chapter 3. Lastly, the Conclusion contains a discussion of the results obtained, followed by a proposal for future work.

2. Background

2.1 Properties of Indium Gallium Nitride

As an electronic material, silicon is far outmatched by III-nitride materials, especially for photovoltaic applications [1], [2]. The III-nitride material system – specifically gallium nitride (GaN), indium nitride (InN), and homogeneous alloys of the two (InGaN) – are direct band gap materials, while Si has an indirect band gap [1], [3]. This fundamental difference in the material properties allows these III-nitride materials to absorb light more efficiently than Si [4]. The advantage provided by the difference in the nature of the material band gap is then compounded when looking at the wavelengths of light which can be absorbed. Si has a band gap of about 1.1 eV, which is relatively low energy in comparison to the maximum of the solar spectrum [2]. This corresponds to optimal light absorption at 1130 nm. The III-Nitrides have band gap energies ranging from 0.7 eV to 3.4 eV, depending on the composition of the InGaN alloy [5]. This means that the materials can be tailored to have optimal light absorption at any wavelength along the most energy dense portion of the available solar spectrum [5], [6]. This relationship is illustrated in Figure 1. In addition to these favorable qualities, III-nitrides have robust photoluminescence, high carrier mobility, high drift velocity, high thermal conductivity, and high temperature and radiation resistance [1], [2]. Each of these qualities can contribute to a robust, high efficiency solar cell.

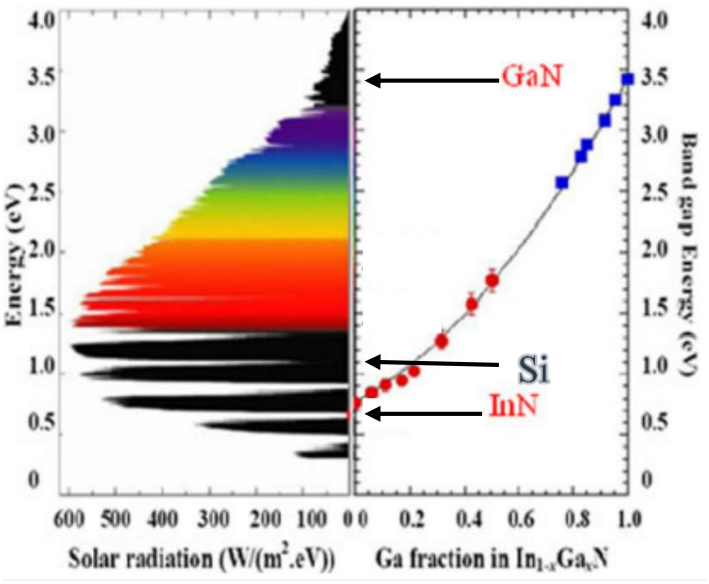

Figure 1. Available energy in the solar spectrum compared to Si and III-nitride band gaps [1].

2.2 Molecular Beam Epitaxy

Molecular beam epitaxy (MBE) is one of many techniques for epitaxial growth – others include metal-oxide chemical vapor deposition (MOCVD), liquid phase epitaxy (LPE), and variations on these. MBE takes place in a specialized vacuum chamber similar to the one described in Figure 2 [7], [8]. The epitaxy relies on chemical bonds forming between one or more vaporized elements and a heated, rotating substrate. The process must be done in ultra-high vacuum to get clean epilayers, and guarantee that the mean free path of particles is larger than the size of the chamber [8].

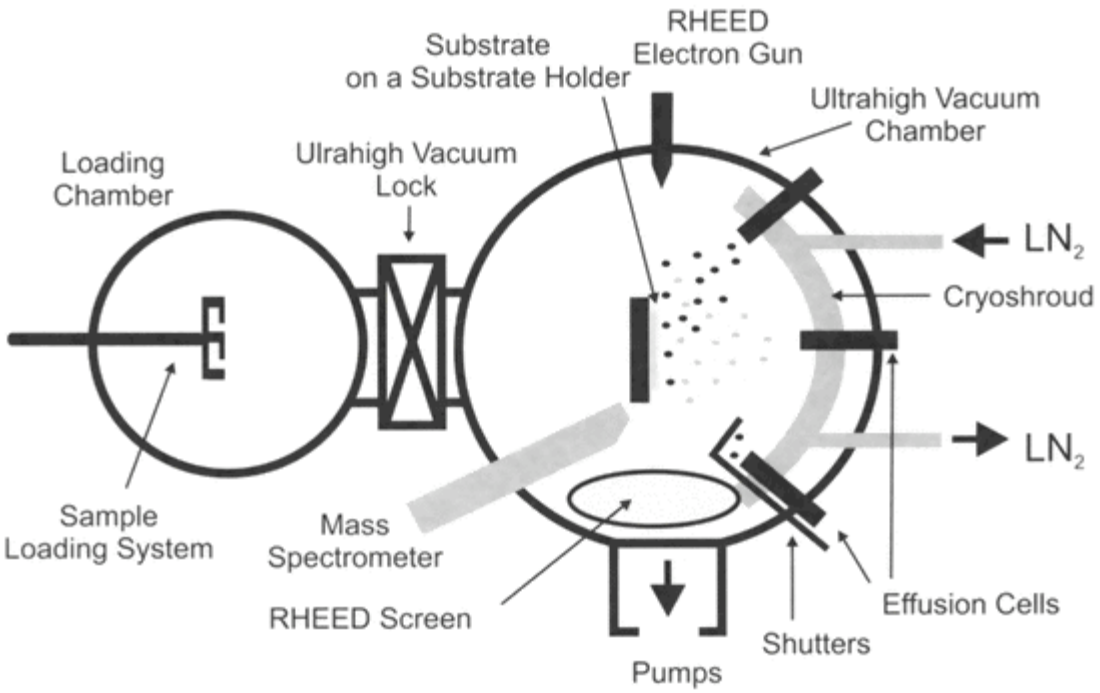

Figure 2. Schematic view of MBE [7].

In MBE, molecular vapor flow rate is a temperature controlled function, so it is a very simple matter to vary material composition as a growth is happening [7], [8]. This property of MBE lends it to use in growing a graded composition material.

2.3 Photoluminescence, Reflectance & Transmittance

Photoluminescence is the process by which light is used to excite electrons in a material. The material may or may not emit light when the excited electrons release their excess energy and relax into equilibrium states [9]. In semiconductor materials, the excited state is the conduction band, and the equilibrium state is the valence band. When subjected to a light spectrum, the photoluminescence of a semiconductor can be used to determine its composition [9]. Reflectance and transmittance can be used to find the same information about a material's composition, but operate on a slightly different physical mechanism. Reflectance is "the ratio of

reflected radiant power to incident radiant power," and transmittance is "the ratio of transmitted radiant power to incident radiant power" [10]. All three measurement techniques record a response at the same wavelength of light, and Equation 1 can be used to calculate the band gap of the material.

$$E_g = \frac{1240}{\lambda} \quad (1)$$

2.4 X-Ray Diffraction

Diffraction is a phenomena that results when every object in a repeating pattern scatters light at specific angles – or constructively interferes with the light. Atoms in a crystalline structure satisfy the requirements of repeating pattern of objects, and the wavelength of x-rays are similar to the distance between atoms. When x-rays are directed at a crystal, they scatter off of the different atomic planes in the material, and create a diffraction pattern that can describe the atomic structure [11]. XRD is typically done by doing what is known as an ω-2Θ curve – to plot the x-ray intensity against the incident angle, ω. This set up is shown in Figure 3.

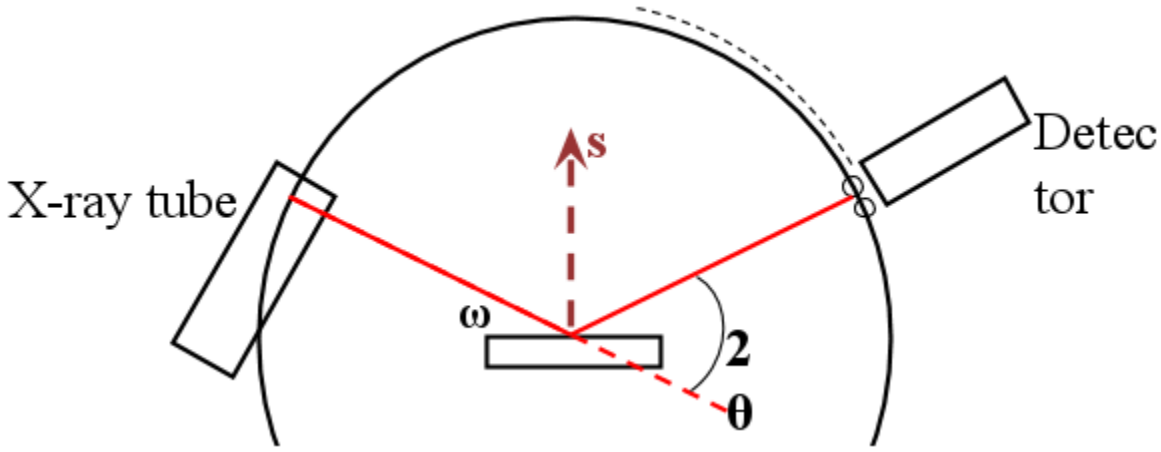

Figure 3. XRD Schematic [11].

X-ray diffraction is useful for finding information about composition, thickness, strain/relaxation, dislocation density, curvature, and more [11].

2.5 Atomic Force Microscopy

AFM is a technique used to measure the roughness of a surface with very high levels of precision. The measurement is done by running a cantilever probe over the surface, while a laser is being deflected off of the back of the probe onto a position sensitive photodetector [12]. This setup is illustrated in Figure 4.

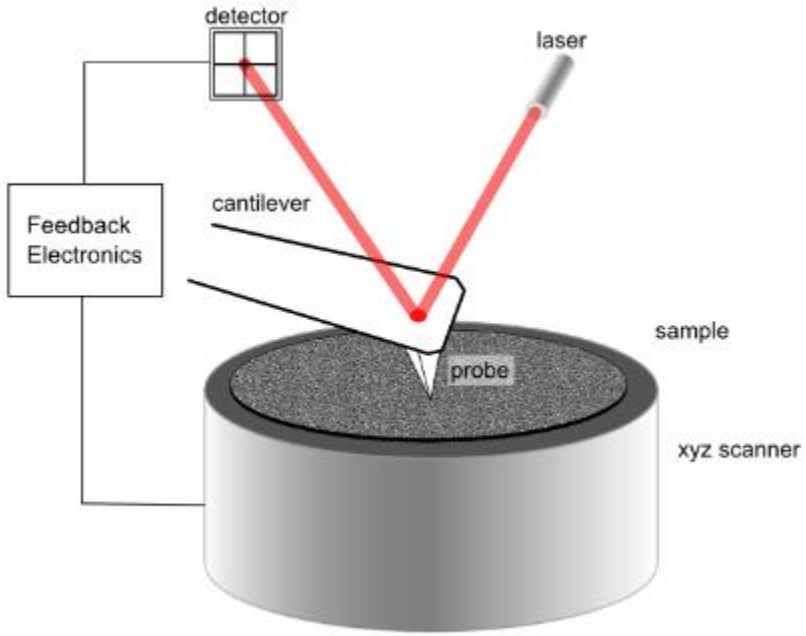

Figure 4. AFM Schematic [12].

AFM is useful for identifying defects and understanding the surface of a crystal.

3. Experimental Approach

3.1 Reference Cell

A reference crystal structure was selected to begin the project. Fabien, et. al. thoroughly investigated an MBE-grown, double-heterojunction (DHJ), InGaN/GaN solar cell in 2016 [13]. With established results to reference, the crystal structure in Figure 5(a) was modified slightly to be that in Figure 5(b). The extra 10nm of p^+-GaN was added to the reference cell clean up the proportions between the layers. Of the InGaN compositions researched in [13], the 20% indium alloy was chosen.

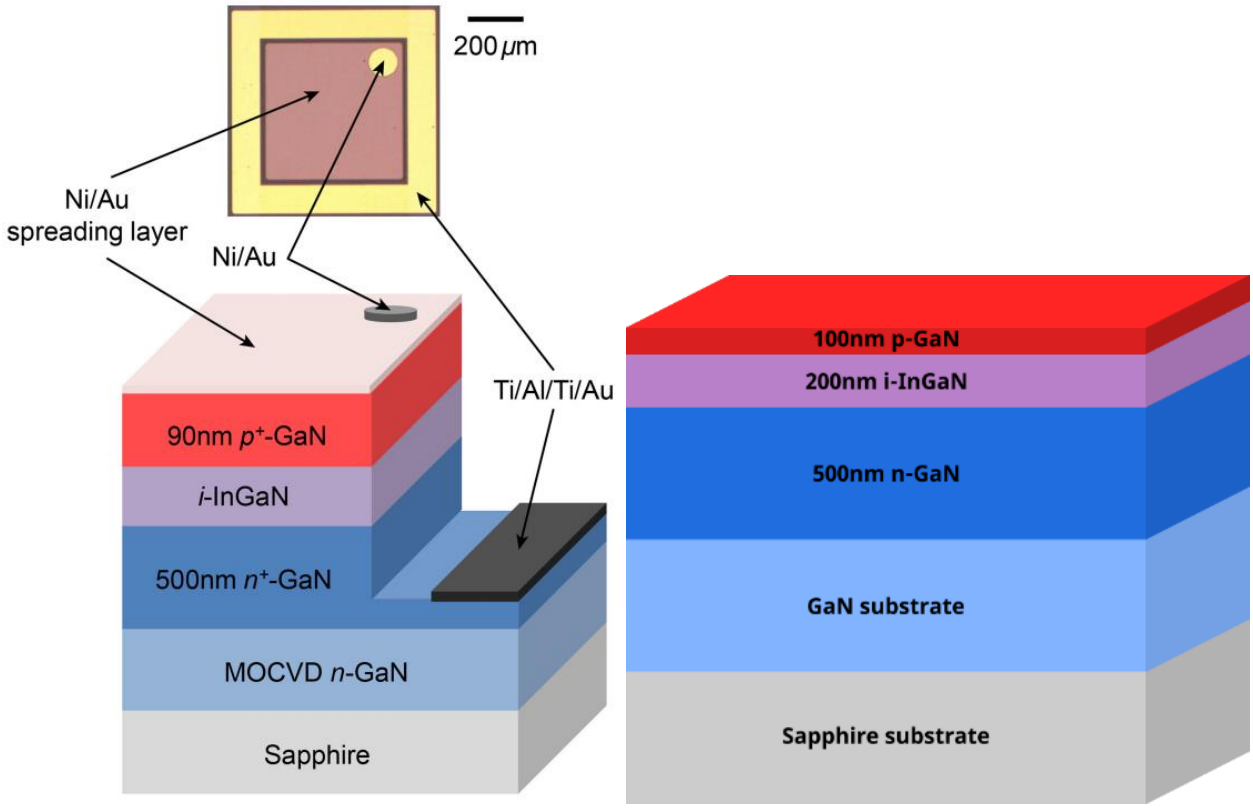

(a) (b)

Figure 5. (a) DHJ structure by Fabien, et. al. [13]. (b) Modified structure used as the reference cell.

A two-inch diameter MOCVD grown *n*-GaN on sapphire substrate was quartered, and one quarter was used to grow the reference crystal. The reference crystal growth was conducted in a Veeco Gen II MBE system shown in Figure 6. As with Fabien's sample, Si was used as the *n*-dopant, and Mg was used as the *p*-dopant. The InGaN layer was not intentionally doped [13]. The growth of the *n*-GaN layer was conducted at a substrate temperature of 800°C. The gallium cell was set to 935°C, and the silicon cell to 1230°C. Both the InGaN and *p*-GaN layers were grown at 600°C. For the InGaN layer, the 20% indium content was achieved by heating the indium cell to 721°C and the gallium cell to 891°C. Finally, the gallium in the *p*-GaN layer was heated to 903°C, and the magnesium dopant valve was set to 150 mils.

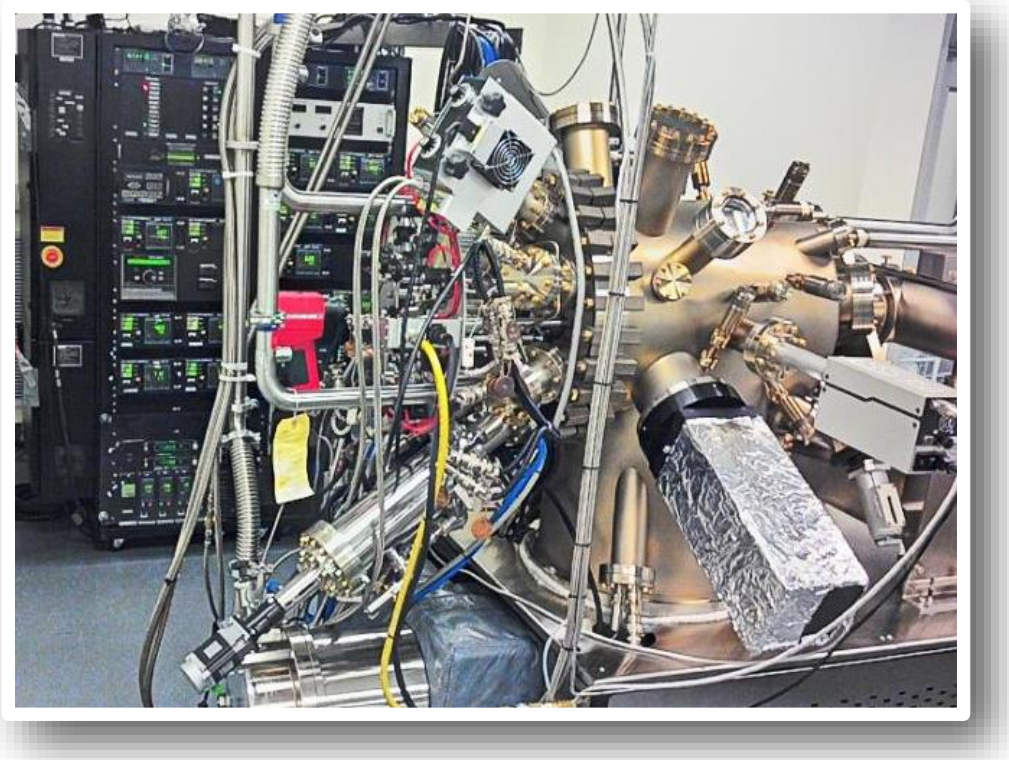

Figure 6. Veeco Gen II MBE System.

Once the sample was grown, it was necessary to examine the crystal and verify that its structure and composition matched the planned structure. To this effect, PL characterization was

done as described in Section 2.4. The PL setup used consisted of a 325nm He-Cd laser with 1mW emission power, a 0.5m-focal-length spectrometer, and a liquid nitrogen cooled Si CCD detector. A portion of this setup is shown in Figure 7. Five PL spectra were recorded at the following temperatures: 15K, 50K, 150K, 250K, and 298K. The sample was cooled on the cold finger of a closed cycle helium cryostat. Each spectrum was taken using an exposure time of 10 seconds and a slit width of 0.5mm.

Figure 7. Photoluminescence Setup.

To further examine the crystal's structure, it was characterized by XRD. These measurements were taken using a Philips X'Pert MRD Diffractometer, shown in Figure 8. High resolution was taken in the 3-axis configuration, while low resolution was taken in order to increase weak signals using the 2-axis configuration.

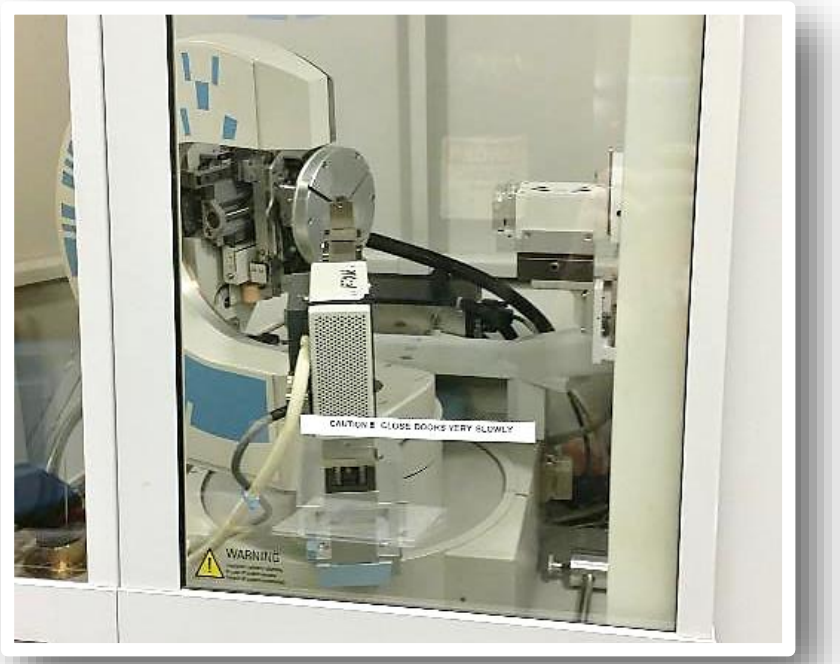

Figure 8. Philips Diffractometer.

Reflectance and transmittance measurements were both taken using a Shimadzu UV-3600 Spectrophotometer shown in Figure 9. These tests were set up with the UVProbe software. The reflectance was taken using a wavelength range of 1200nm down to 300nm, at a medium scan speed, and with a 1nm sampling interval. The spectrophotometer slit width was set to 2nm, and direct detection was used. The grating was set to change when the scan reached 760nm, and the light source changed at 310nm. The detector was set to change at 1650nm and 850nm. Two reflectance scans were taken with these settings. Five transmittance measurements were taken with a similar set up. Each scan used a different combination of range, scan speed, and sampling interval. The first scan was taken from 3300nm to 190nm at a fast speed with a 1nm interval, this was followed by a scan from 1200nm to 190nm at the same speed and interval as the range was narrowed in on the interval of interest. The last three scans were taken from 650nm to 250nm. The first and second of these were done at a medium speed, while the third was taken at a slow

speed. An interval of 1nm was used for the first of the three scans, and this interval was reduce to 0.5nm and 0.2 for the last two, respectively.

Figure 9. Shimadzu UV-3600 Reflectance Setup.

After thorough investigation of the material composition with the four methods described above, the crystal was subject to AFM in order to examine its surface before it was processed into a solar cell. The AFM was performed using a Bruker Dimension 3000 Atomic Force Microscope shown in Figure 10, using a Si cantilever with a 10nm radius of curvature in tapping mode.

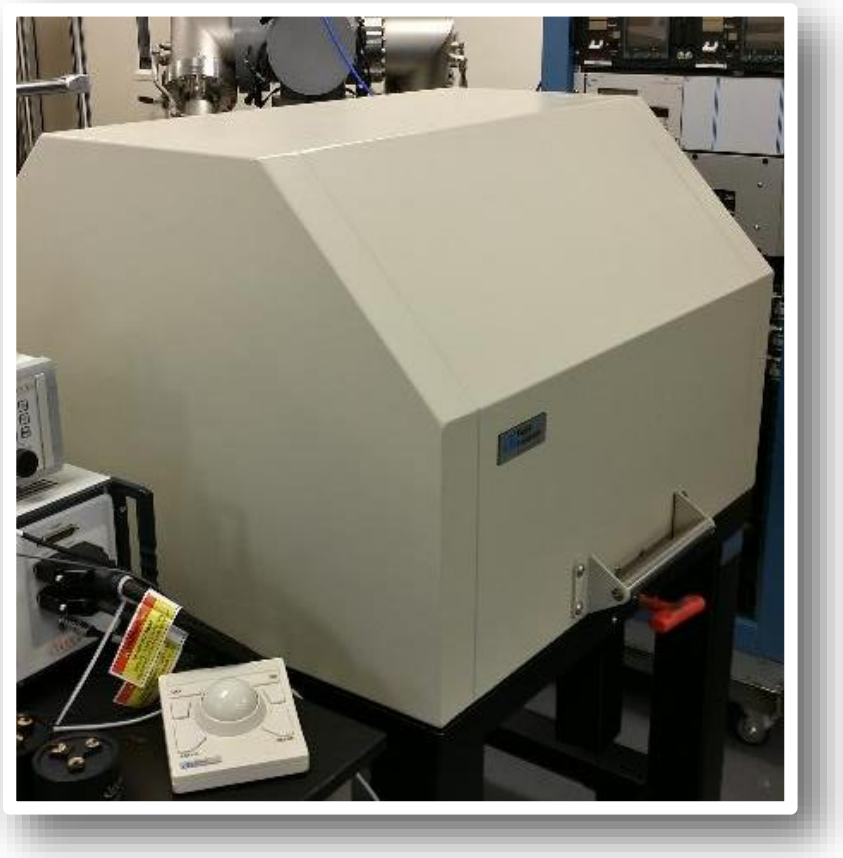

Figure 10. Bruker AFM.

Once the structural characterization was completed, the crystal was prepared for processing. First, the adhesive used for PL was removed by thoroughly scrubbing the back of the sample with a cotton swab soaked in acetone, followed by a methanol rinse, and an IPA rinse. Next, the titanium back was etched off of the substrate. The crystal was submerged in HCl as detailed in Table 1 to etch away the titanium. The black bars in Table 1 indicate when the sample was removed from the etch to be re-cleaned with acetone, methanol, and IPA.

Table 1. Titanium Etch Times.

Etch Number	1	2	3	4	5	6	7	8	9	10	11	12	13	14
Time [min]	1	1	1	2	2	3	5	3	3	5	5	5	3	3

Once the titanium was etched, the crystal was processed into several solar cell devices as follows. Photoresist was spun onto the top surface – the *p*-GaN layer – of the substrate. The

crystal then underwent several photolithography steps of spin-coating – exposing – developing – "processing" and - cleaning using the mask set shown in Figure 11. Here, the center mask is used first to define the central mesas of the devices. Then the mask on the right is used to define the contact on top of the mesa, and the mask on the left was used to define the back contacts of the devices concentric to the top contacts.

Figure 11. Solar Cell Mask Set.

The processing step mentioned above is different for each mask. For the mesa formation, the samples were etched using a combination of Cl_2 and BCl_3 gases in an inductively coupled reactive ion etch system. For each of the contact formation steps, the developed areas were exposed to metal in an electron beam evaporator using layers of Ni and Au for the p-type top contacts and Ti and Au for the n-type back contacts as shown in Figure 5(a).

At this point the solar cell was completely fabricated and ready to be connected to the electrical testing station. The reference solar cell was placed under a solar lamp with an output of about $1000W/m^2$. A probe station and source-measure unit were used to find the I-V curves for each device.

3.2 Graded Layer Cell

With the reference cell fully characterized, work could begin on the graded layer cell. Again, the first step was to choose a structure. The main objectives in choosing this structure were to keep it as consistent with the reference cell as possible, and to also incorporate a compositionally graded InGaN layer. With these goals in mind, only the InGaN layer of the reference cell structure in Figure 5(b) was modified. The thickness of this layer was left at 200nm, but instead of a constant alloy composition of 20% indium, a linear grade from 25% indium at the *n*-GaN interface to 15% indium at the *p*-GaN interface. This structure allowed the experimental crystal to maintain an average alloy composition of 20% indium while containing a graded layer. The graded layer cell structure can be seen in Figure 12.

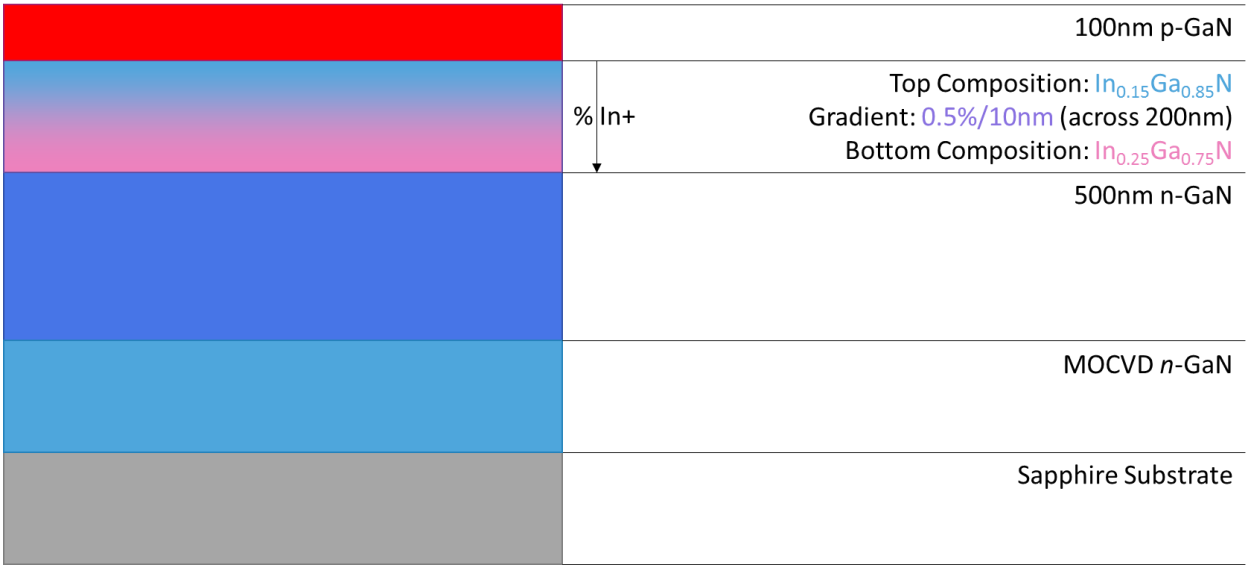

Figure 12. Graded Cell Structure.

Because of the similar structure to the reference cell, the growth of the graded layer crystal was identical to the growth of the reference crystal, except for the InGaN layer. The graded layer was grown by heating the gallium to 917°C, and the indium to 731°C. These temperatures were then subjected to a linear ramp over the growth period, and ended at 924°C and 709°C, respectively.

This sample's structure was first examined with high resolution XRD, similar to the reference cell. A 3-axis measurement inconclusively found weak traces of the InGaN from the graded layer, so a low resolution 2-axis measurement was taken in order to increase the signal from the sample well above the noise. Once the XRD data was gathered, the reflectance of the graded layer crystal was measured using the same parameters that were used for the reference cell. Finally, the surface of the graded layer crystal was examined with AFM, also with exactly the same set up as the reference cell.

4. Experimental Results

4.1 Reference Cell

The photoluminescence spectra at three different points (point 1, left frames; point 2, center frames; and point 3, right frame) on the crystal at each temperature can be seen in the following figures. It should be noted that generally, the PL peak shifts to higher energy (shorter wavelength) as the temperature decreases, while the intensity increases dramatically especially at the lowest temperatures. The material present in the crystal could be determined by examining the location of each peak in Figure 13 applying Equation 1 and comparing this with published data characterizing the bandgap energy as a function of composition. The first peak in intensity occurs at a wavelength of about 360nm, and the second peak is located at 480nm. Another very small peak can be found at 610nm. The band gap energies for each peak are 3.45eV, 2.58eV, and 2.03eV respectively. The first peak matches reasonable well with GaN, which has a band gap of 3.4eV, and the 2.58eV peak falls within the expected range of 0.65eV to 3.4eV for InGaN alloys. At this point, it appeared that all of the material that was intentionally added to the crystal had been detected, so the third peak came as a slight surprise. However, it was determined that the 2.03eV was due to defects states which exist in the GaN films.

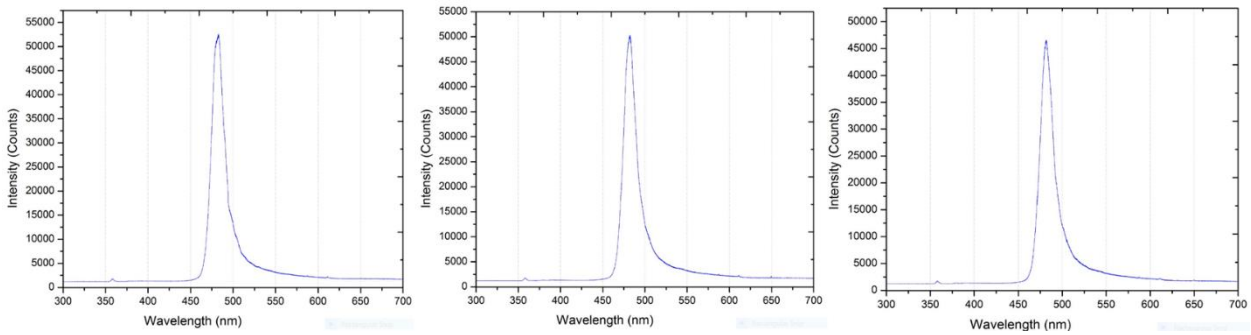

Figure 13. Photoluminescence at 15K.

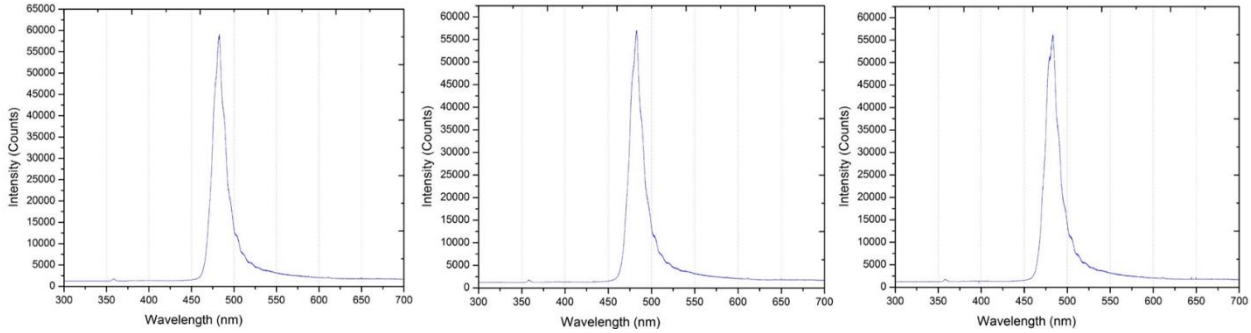

Figure 14. Photoluminescence at 50K.

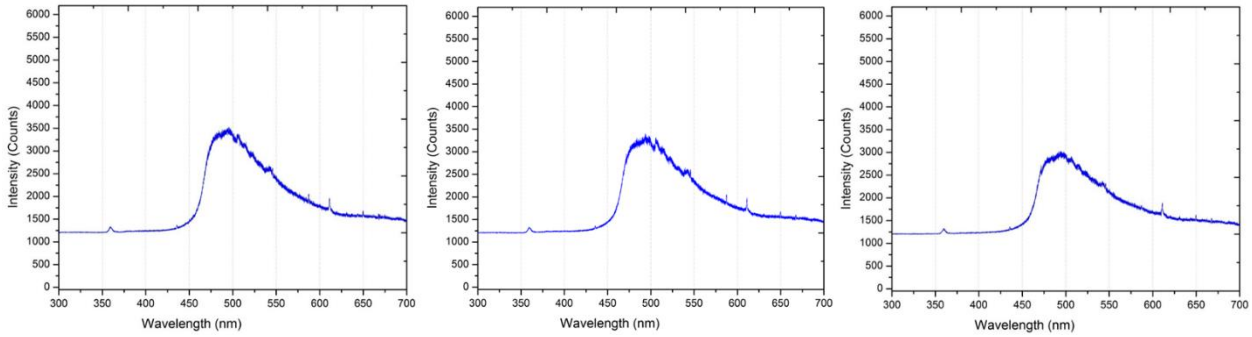

Figure 15. Photoluminescence at 150K.

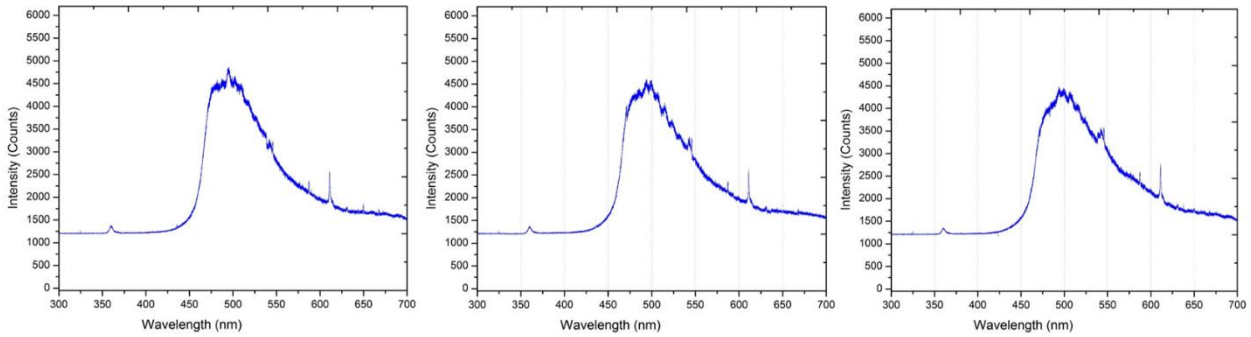

Figure 16. Photoluminescence at 250K.

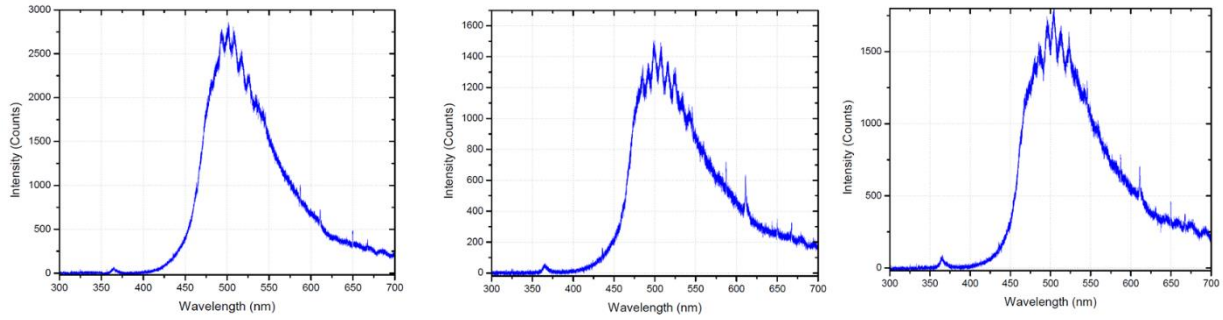

Figure 17. Photoluminescence at 298K.

The ω-2Θ scan obtained from x-ray diffraction is shown in Figure 18. The rightmost peak is due to AlN in the as-purchased substrate, while the other two peaks can be matched to the expected materials – InGaN and GaN – as shown in the figure by their respective lattice constants.

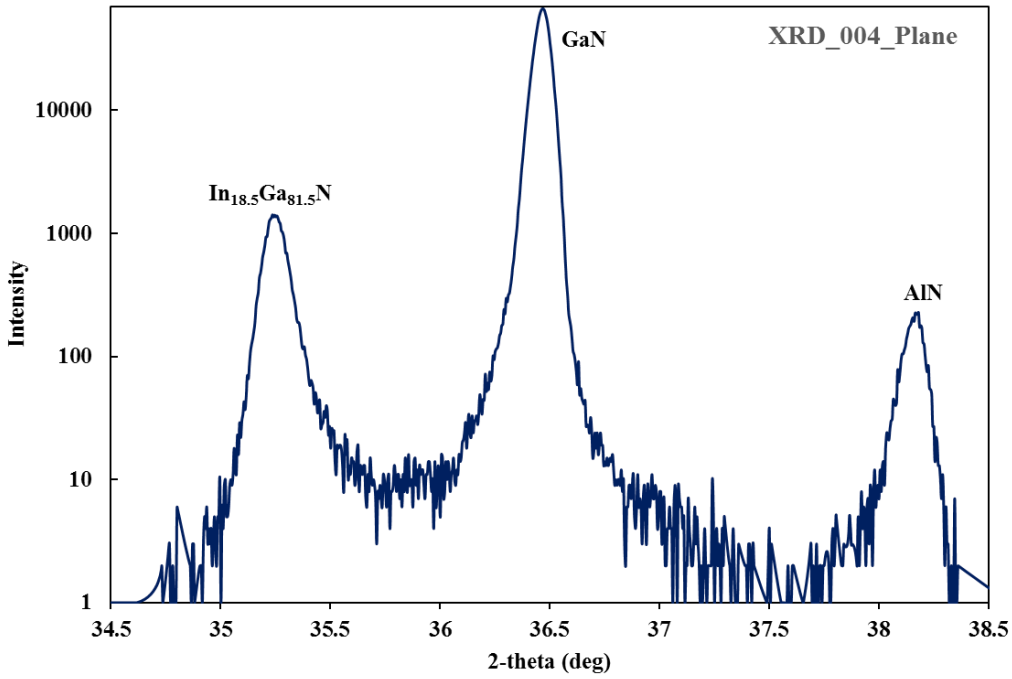

Figure 18. Reference Crystal ω-2Θ Scan.

A reciprocal space map of the InGaN reference solar cell structure was also obtained from XRD. This result is presented in Figure 19. Generally, there are two main features here. The top "spot" and the bottom "spot." The top spot, is from the InGaN film which was grown, and the bottom spot results from x-ray diffraction from the GaN substrate. The most important parameter to derive, if only qualitatively, is the in-plane lattice parameter of the grown film. This is directly related to the horizontal position of the spot within the scan window. Here we see that the horizontal positions of both spots are aligned within the window. This is a direct indication

that the lattice of the grown crystal is completely strained to the lattice of the substrate, and no new dislocations are formed due to strain buildup during crystal growth.

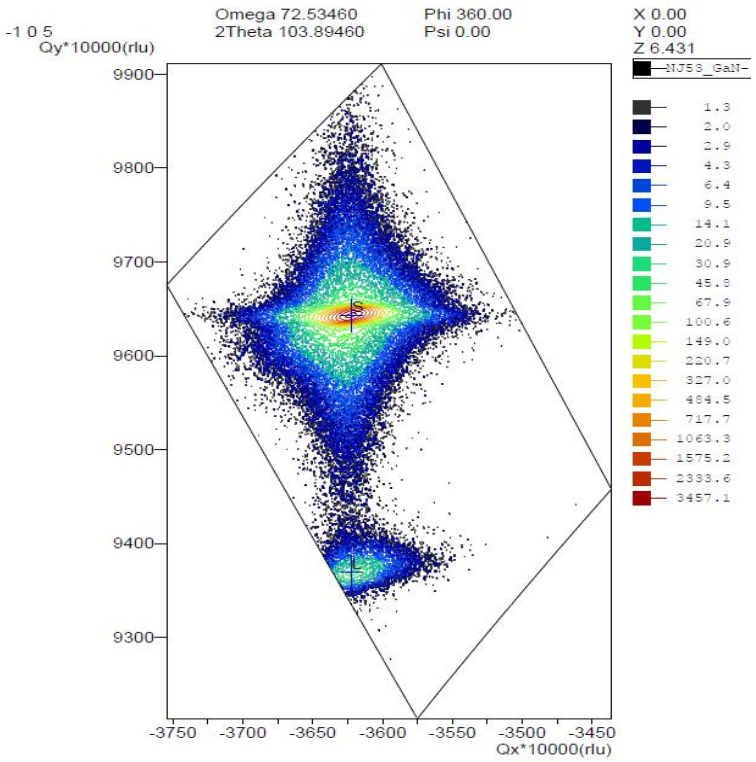

Figure 19. Reference Crystal Reciprocal Space Map.

Figure 20 shows the reflectance profile for the reference crystal. Figure 21 shows an easier-to-interpret form of the same data, a plot of the rate of change of reflectance with respect to the wavelength. The sharp transitions in reflectance indicate the sudden influence of a different material from a different layer within the structure. These transitions appear as extrema in the plot of the derivative. As is shown in Figure 21, the reflectance of the crystal changes at 366nm and again at 483nm. Similarly to the procedure for analyzing PL data, Equation 1 was applied, and the materials influencing reflectance were shown to have band gap energies of 3.38eV and 2.56eV. These match the results obtained from PL within a reasonable margin, and the material can be said to consist of GaN and InGaN once again. Figure 22 shows the transmittance measurements of the interval of interest – 650nm to 250nm. In the same way that

they do with the reflectance of a crystal, sharp transitions in the transmittance indicate that a material is in that crystal. The data points displayed in Figure 22 are very similar to those found from both PL and reflectance measurements. Using the same analysis as before, the transmittance data reinforces the understanding of the materials found in the reference crystal.

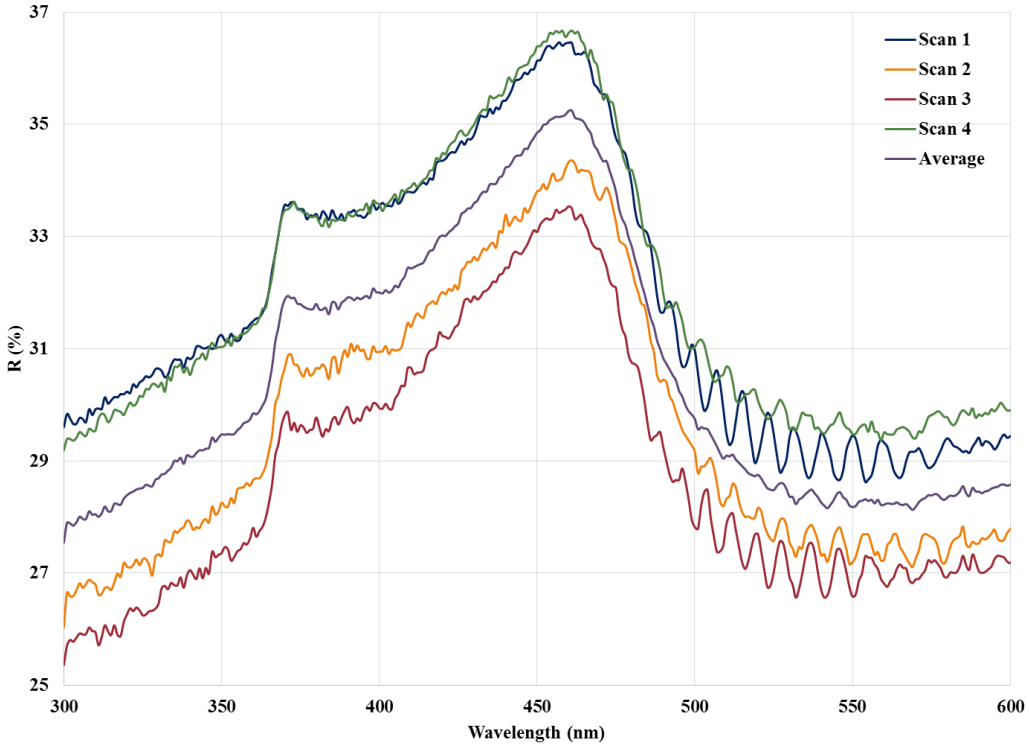

Figure 20. Reflectance Profile of Reference Crystal.

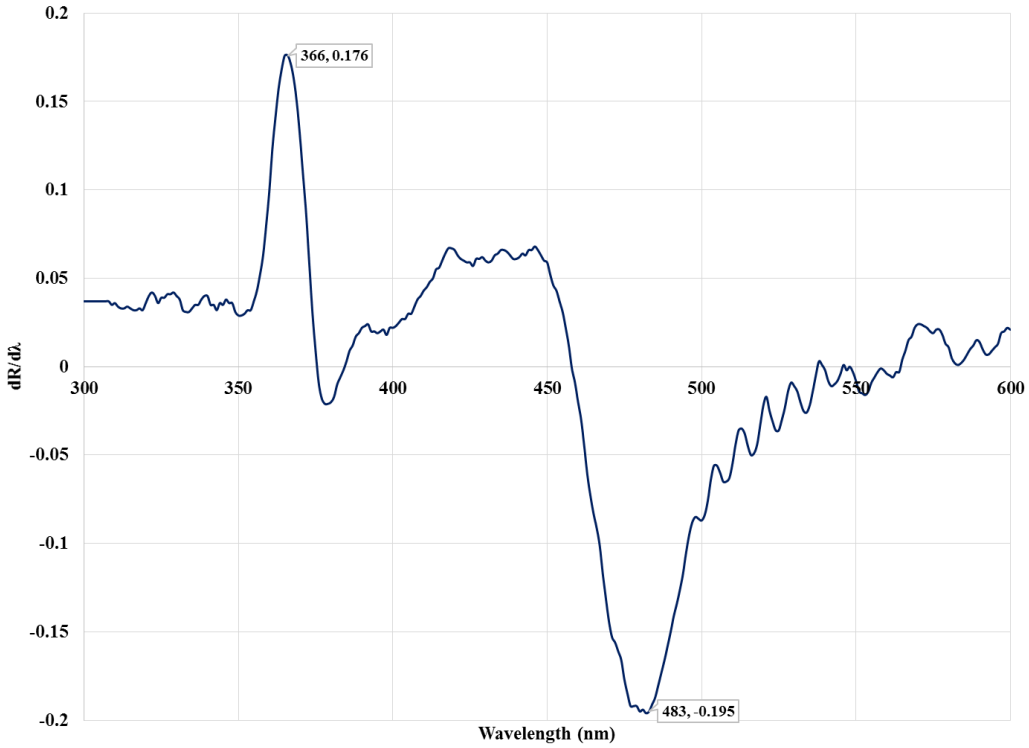

Figure 21. Derivative of Reflectance for Reference Crystal.

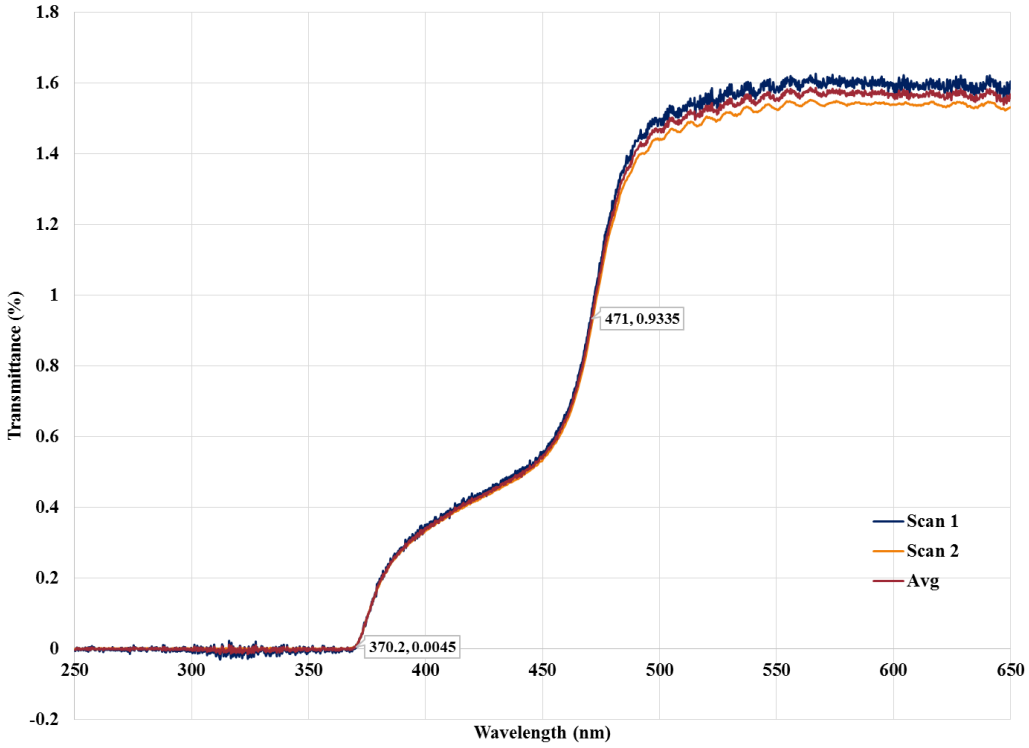

Figure 22. Transmittance of Reference Crystal.

The surface of the crystal was characterized at multiple points, but to understand the surface, only one sample of the available AFM data was examined. This point is near the middle of the substrate, and Figure 23 shows the same data before and after software filtering, and Figure 24 displays a larger area containing the region in Figure 23. At first glance, Figure 23(a) appears to be a much smoother portion of the surface than Figure 23(b). However, this is just an artifact of atomic force microscopy. The dark regions at the top and bottom of Figure 23(a) are a telltale sign that the data shown is distorted by the arc that the AFM tip follows when collecting this data. To remove this artifact, the image can be "smoothed" in WSxM, and the result is Figure 23(b). The flattened image is much easier to interpret than the indistinct raw data. Figure 23(b) shows a 5-µm square region of the crystal surface with many pits at a density of approximately 1-5 per µm. This is an expected result, since all III-nitride materials have high defect density, and because they are also very tolerant of defects, this result does not have any negative effects on the project [14]. Figure 24 shows that the larger area consists of reasonably similar surface material, and leads to the conclusion that this crystal is high enough quality to use as a solar cell.

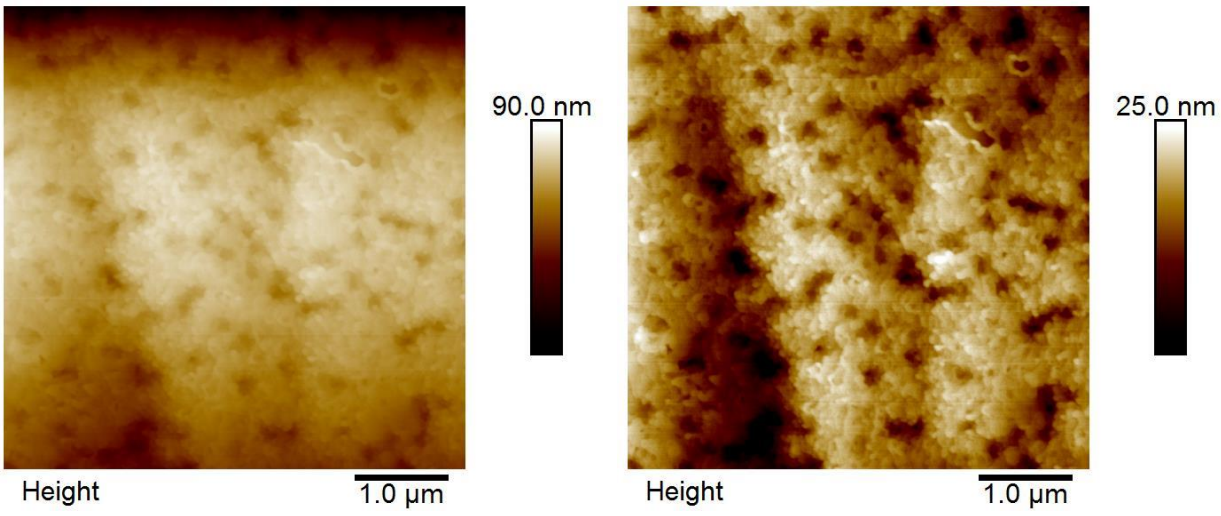

Figure 23. Middle 25-µm^2 AFM (a) raw data. (b) software-flattened image.

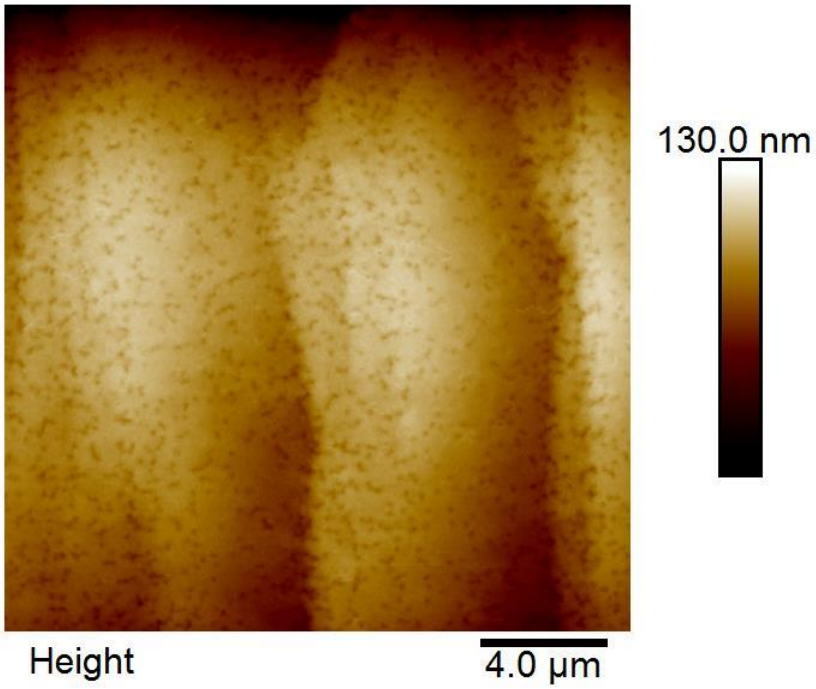

Figure 24. Middle 400-µm^2 AFM.

The absolute current was plotted against voltage for each device. An example of this plot is displayed in Figure 25. In this semilog plot, Tshe minimum point of each curve represents the open-circuit voltage for the device, and where the curve crosses the y-axis represents the device's short-circuit current. The non-zero V_{OC} for the dark measurements is an artifact of the data acquisition system. For the device in Figure 25, V_{OC} is 0.03V and I_{SC} is 1.74µA. This information was taken from each device and recorded in Table 2.

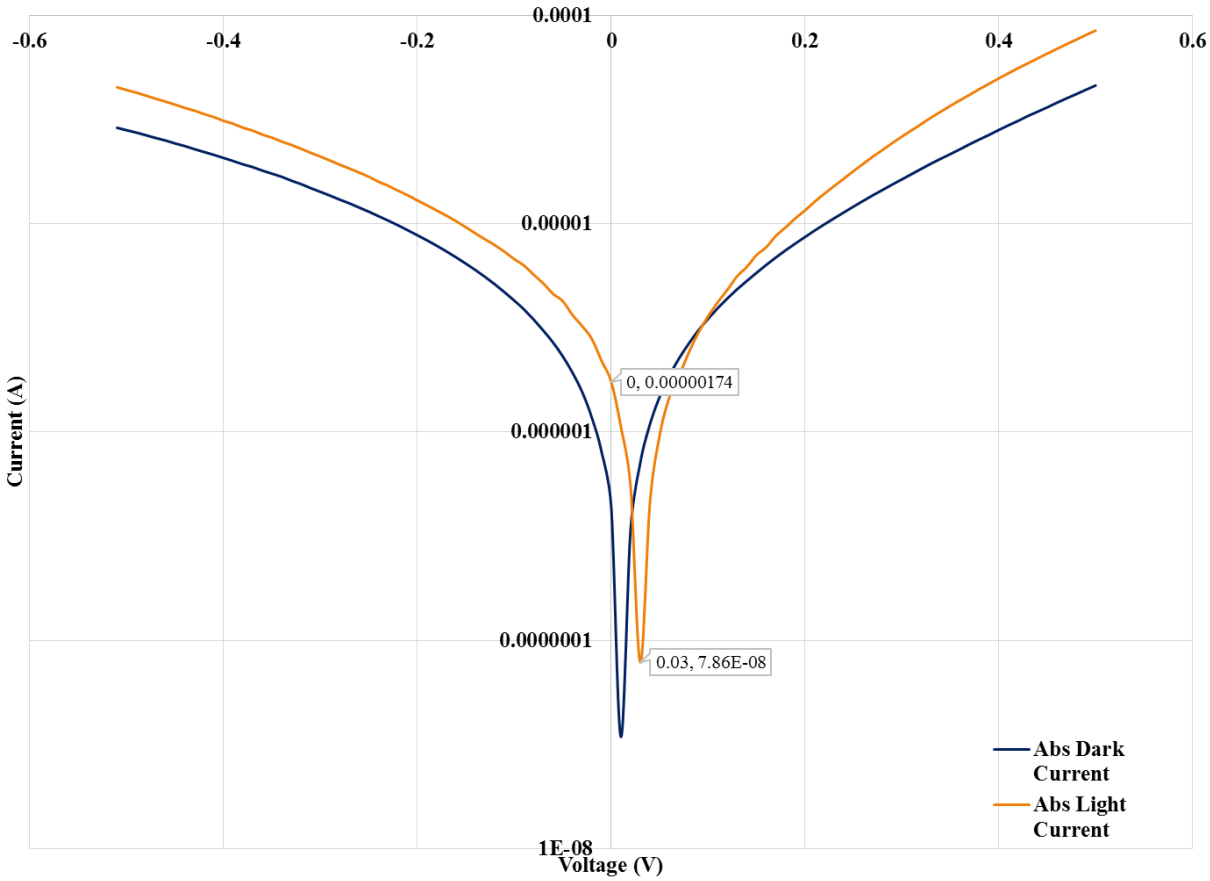

Figure 25. I-V Plot – Reference Device C2R4.

Table 2. Reference Device Power Metrics.

Device	V_{OC} [V]	I_{SC} [µA]
C1R2	0.01	20.3
C1R3	0.01	6.0
C1R4	-0.08	4.7
C1R5	0.01	3.1
C2R1	0.01	7.5
C2R2	0.01	5.7
C2R3	0.01	1.9
C2R4	0.03	1.7

4.2 Graded Layer Cell

The 2Θ-ω scan obtained from x-ray diffraction on the graded layer cell is shown in Figure 26. Similar to the results from the reference cell, the rightmost peak is due to the AlN in the substrate, while the other two peaks can be matched to the expected materials – InGaN and GaN. The high resolution 3-axis measurement, shown here in blue, was unable to detect any indium in the sample, so the 2-axis measurement was taken to increase the intensity at the expense of resolution. From the 2-axis plot it is obvious that both InGaN and GaN are present, but no other information about the composition can be determined analytically due to the complex nature of the graded InGaN layer. A key difference between Figure 26 and Figure 18 is the intensity of the InGaN peak. There is a nearly two-orders-of-magnitude swing from one to the other, and the reason for this is still a subject of investigation.

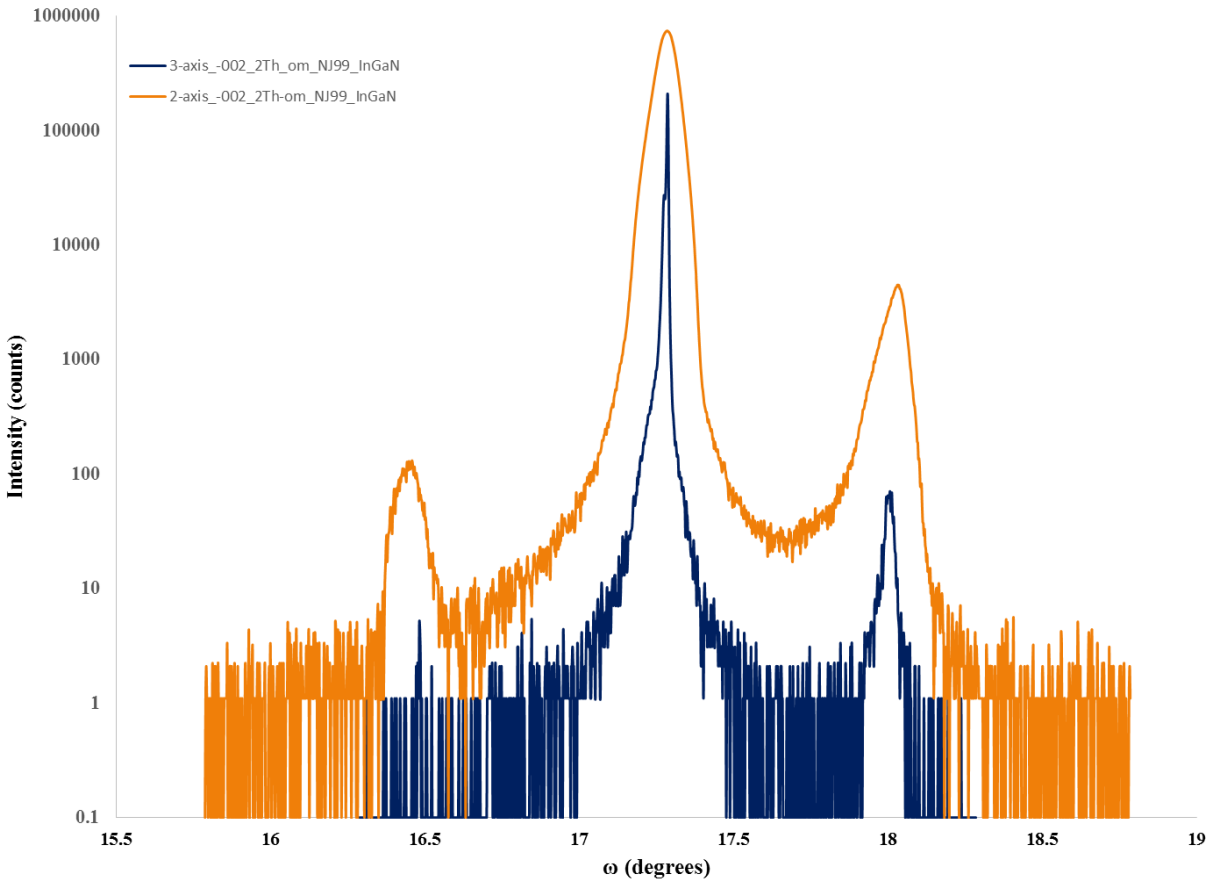

Figure 26. Graded Layer 2Θ-ω Scan.

The data obtained from XRD was not sufficient to conclude anything about the composition of the graded layer crystal, so reflectance data was gathered for this crystal as well. The reflectance of this sample is shown in Figure 27, and its derivative in Figure 28. When compared with the reflectance data for the reference device, it becomes very obvious that there is an entire feature missing from this crystal. The feature due to GaN (at about 360nm) is still present in both versions of the reflectance data, but there is no immediately obvious feature for InGaN. We may generally assume that the sudden dampening of the high frequency oscillations at shorter wavelengths than ~450nm is due to the absorption of the graded InGaN layer, but more detailed studies will need to be performed.

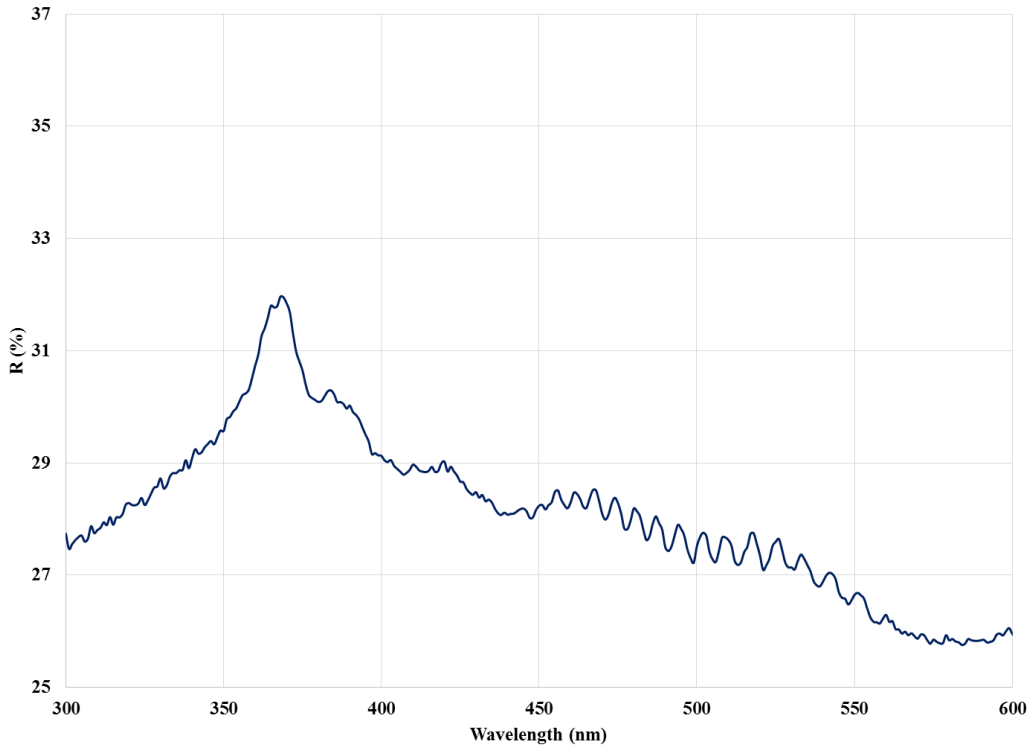

Figure 27. Reflectance of Graded Layer Crystal.

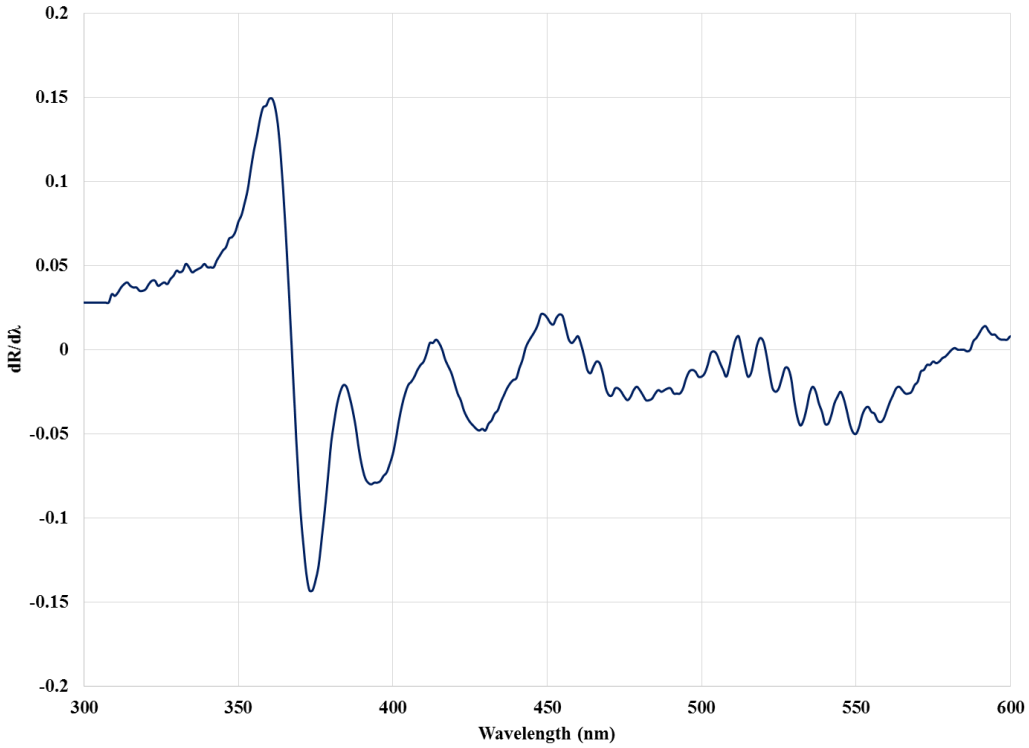

Figure 28. Derivative of Reflectance for Graded Layer Crystal.

The surface of this crystal was also examined. This was done with AFM, similar to the reference crystal, and the results are presented in Figure 29. The most apparent difference between the AFM results presented here and those presented with the reference crystal is the lack of deep holes in this surface. In all three images, it seems as if material is actually protruding from the surface. This could be due to a few different things, but the most likely of them is a consequence of the state of the crystal at the time of AFM. These measurements were taken after growth, but before the crystal was cleaned. Any excess metal in the growth chamber could have easily been deposited on the surface in the form of "droplets," obscuring an otherwise ordinary surface underneath. Much more optimistic explanations of these results might suggest that the graded layer provided a perfect avenue for lattice strain, and virtually eliminated defects.

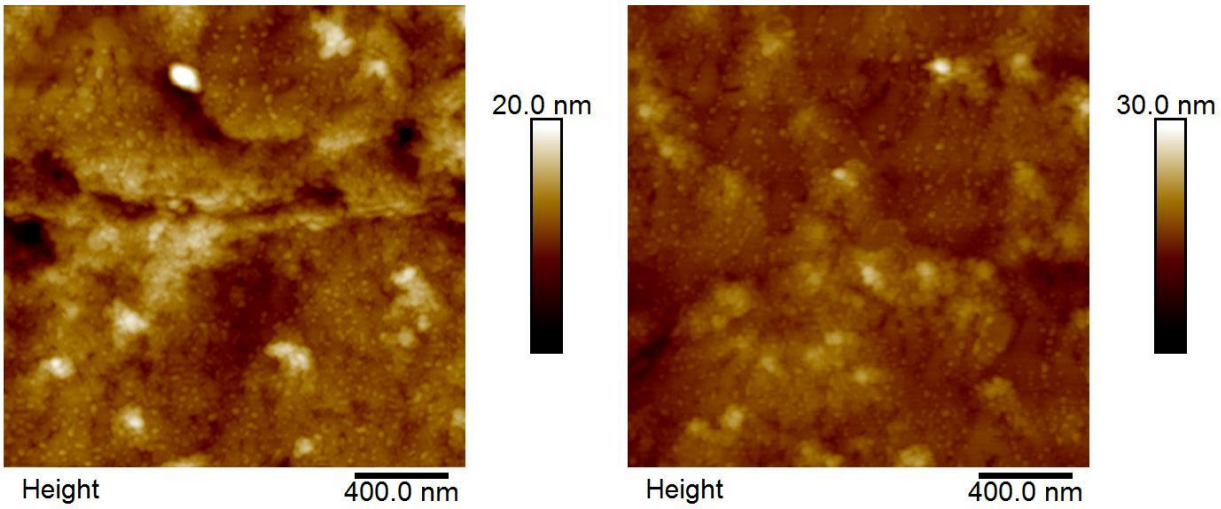

Figure 29. Graded Layer 4-μm^2 AFM Results.

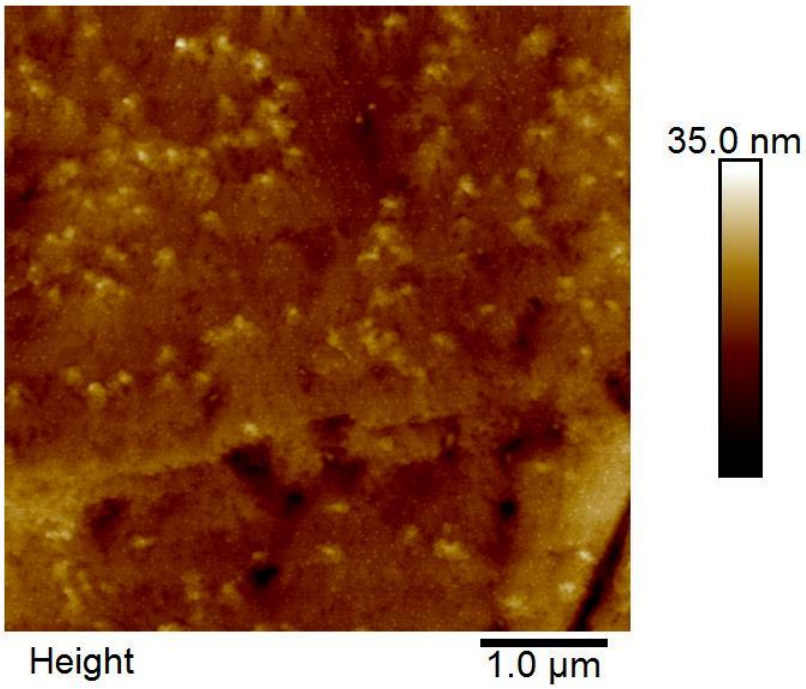

Figure 30. Graded Layer 25-μm^2 AFM Results.

5. Conclusions

5.1 Discussion of Results

The solar cell structures presented in this thesis are far from optimized, and a lot of work still remains to fully understand the graded layer crystal. The structural design and characterization of a P-i-N, double-heterojunction solar cell and a graded layer crystal for use in solar devices was completed. Additionally, a preliminary optical and electrical characterization was completed for the P-i-N, double-heterojunction cell.

With respect to the reference device, the results of the growth were as expected. Four different characterization techniques confirmed that the fabricated device matched the design. X-ray diffraction further revealed that the InGaN layer was strained to GaN in the crystal, resulting in fewer defects than the alternative. Examination of the surface with atomic force microscopy revealed a standard number of defects consistent with a typical III-nitride crystal. On the other hand, the graded layer crystal was not so straightforward. There are conflicting results from the XRD and reflectance measurements about whether the crystal contains indium. The surface of the graded layer sample is also atypical. Further study is required to fully understand the graded layer device, and get it to a point where it can be used as a solar cell.

5.2 Suggestions for Future Work

The most pressing question that arose from this research is whether or not the graded layer crystal contained indium. Future research should first focus on determining whether or not the indium is present. Regardless of the answer to this question, the next question to ask is “Why?”. Why was there no indium present? Or why did it take so much more effort to detect the indium? Alongside this investigation, it would be beneficial to clean the crystal, and re-measure

the surface in order to determine why the AFM results were so odd. Once all of the structural characterization is completed and understood, the logical next step would be to process the crystal into several solar devices and characterize them optically and electrically, just like what was done with the reference crystal. Once the graded layer device finished this process, it would be a perfect baseline for future studies on optimizing structural and growth parameters in pursuit of high efficiency III-nitride solar cells.

References

[1] A. G. Bhuiyan, K. Sugita, A. Hashimoto, and A. Yamamoto, "InGaN Solar Cells: Present State of the Art and Important Challenges," *IEEE J. Photovolt.*, vol. 2, no. 3, pp. 276–293, Jul. 2012.

[2] Y. K. Kuo, J. Y. Chang, and Y. H. Shih, "Numerical Study of the Effects of Hetero-Interfaces, Polarization Charges, and Step-Graded Interlayers on the Photovoltaic Properties of (0001) Face GaN/InGaN p-i-n Solar Cell," *IEEE J. Quantum Electron.*, vol. 48, no. 3, pp. 367–374, Mar. 2012.

[3] M. Z. Alom, M. S. Hasan, M. R. Islam, I. M. Mehedi, and A. M. Dobaie, "Estimation of minority carrier lifetime in InGaN single junction solar cell," in *2015 International Conference on Electrical Electronic Engineering (ICEEE)*, 2015, pp. 257–260.

[4] J. Wu, "When group-III nitrides go infrared: New properties and perspectives," *J. Appl. Phys.*, vol. 106, no. 1, p. 11101, Jul. 2009.

[5] D. Y. Zhang, X. H. Zheng, L. J. Tang, J. R. Dong, H. Wang, and H. Yang, "Photovoltaic Effects of InGaN/GaN Double Heterojunctions With p-GaN Nanorod Arrays," *IEEE Electron Device Lett.*, vol. 31, no. 12, pp. 1422–1424, Dec. 2010.

[6] J. K. Sheu *et al.*, "Demonstration of GaN-Based Solar Cells With GaN/InGaN Superlattice Absorption Layers," *IEEE Electron Device Lett.*, vol. 30, no. 3, pp. 225–227, Mar. 2009.

[7] N. N. Ledentsov, Ed., "Basics of MBE growth," in *Growth Processes and Surface Phase Equilibria in Molecular Beam Epitaxy*, Berlin, Heidelberg: Springer Berlin Heidelberg, 1999, pp. 3–32.

[8] F. Rinaldi, "Basics of Molecular Beam Epitaxy (MBE)," University of Ulm, Annual Report, 2002.

[9] R. Ye and A. Barron R., "Photoluminescence Spectroscopy and its Applications," *OpenStax-CNX*, vol. m38357.

[10] "Reflection, Transmission, and Absorption." [Online]. Available: http://light-measurement.com/reflection-absorption/. [Accessed: 28-Apr-2017].

[11] S. A. Speakman, "Introduction to High Resoluton X-Ray Diffraction of Epitaxial Thin Films," Massachusetts Institute of Technology.

[12] "AFM Beginner's Guide." [Online]. Available: http://afmhelp.com/index.php?option=com_content&view=article&id=51&Itemid=57. [Accessed: 28-Apr-2017].

[13] C. A. M. Fabien, A. Maros, C. B. Honsberg, and W. A. Doolittle, "III-Nitride Double-Heterojunction Solar Cells With High In-Content InGaN Absorbing Layers: Comparison of Large-Area and Small-Area Devices," *IEEE J. Photovolt.*, vol. 6, no. 2, pp. 460–464, Mar. 2016.

[14] S. J. Pearton, J. C. Zolper, R. J. Shul, and F. Ren, "GaN: Processing, defects, and devices," *J. Appl. Phys.*, vol. 86, no. 1, pp. 1–78, Jul. 1999.